JOURNAL OF GEOPHYSICAL RESEARCH, VOL. 112, G04S44, doi:10.1029/2006JG000297, 2007

Arctic tundra shrub invasion and soot deposition: Consequences for spring snowmelt and near-surface air temperatures

John E. Strack,[1] Roger A. Pielke Sr.,[1] and Glen E. Liston[2]

Received 23 August 2006; revised 9 April 2007; accepted 3 May 2007; published 2 November 2007.

[1] Invasive shrubs and soot pollution both have the potential to alter the surface energy balance and timing of snow melt in the Arctic. Shrubs reduce the amount of snow lost to sublimation on the tundra during the winter leading to a deeper end-of-winter snowpack. The shrubs also enhance the absorption of energy by the snowpack during the melt season by converting incoming solar radiation to longwave radiation and sensible heat. Soot deposition lowers the albedo of the snow, allowing it to more effectively absorb incoming solar radiation and thus melt faster. This study uses the Colorado State University Regional Atmospheric Modeling System version 4.4 (CSU-RAMS 4.4), equipped with an enhanced snow model, to investigate the effects of shrub encroachment and soot deposition on the atmosphere and snowpack in the Kuparuk Basin of Alaska during the May–June melt period. The results of the simulations suggest that a complete invasion of the tundra by shrubs leads to a 2.2°C warming of 3 m air temperatures and a 108 m increase in boundary layer depth during the melt period. The snow-free date also occurred 11 d earlier despite having a larger initial snowpack. The results also show that a decrease in the snow albedo of 0.1, owing to soot pollution, caused the snow-free date to occur 5 d earlier. The soot pollution caused a 1.0°C warming of 3 m air temperatures and a 25 m average deepening of the boundary layer.

Citation: Strack, J. E., R. A. Pielke Sr., and G. E. Liston (2007), Arctic tundra shrub invasion and soot deposition: Consequences for spring snowmelt and near-surface air temperatures, *J. Geophys. Res.*, *112*, G04S44, doi:10.1029/2006JG000297.

1. Introduction

[2] There is growing evidence that the size and number of deciduous shrubs (dwarf birch "*Betula nana*," willow "*Salix* sp.," and green alder "*Alnus crispa*") in arctic Alaska is increasing due to the recent warming in this region [*Tape et al.*, 2006; *Sturm et al.*, 2001a]. Through an analysis of numerous aerial photograph pairs, *Tape et al.* [2006] found an average relative increase in shrub coverage of 33% and 160% for slopes and river terraces/floodplains, respectively, over the past 50 a. In addition, *Goetz et al.* [2005] have used satellite data to detect an increase in photosynthetic activity in Alaskan and Canadian tundra over the past 22 a.

[3] Soot deposition in the Arctic has the potential to increase in future years owing to increased human activity (energy extraction and ocean shipping) in the region [*Hansen and Nazarenko*, 2004]. Soot lowers the albedo of the snowpack, leading to enhanced absorption of solar radiation. Since there has already been pronounced warming at high latitudes and future warming is expected to be most extreme in these regions, it is of utmost importance to develop a thorough understanding of the processes governing Arctic climate. The goal of this work is to determine the amount of regional warming that could be expected from either a near total replacement of the tundra with shrubs or with increased Arctic soot deposition.

[4] The coverage of shrubs in this region is very important because of their strong impact on snow distributions. Observations by *Sturm et al.* [2001b] and *Pomeroy et al.* [2006] illustrate the effect shrubs have on snow accumulation in the Arctic. Snow depth is increased significantly in the presence of these shrubs because they reduce the wind speed, which leads to local accumulation of blowing snow. In addition, since snow particles that are captured in these shrub regions are less likely to become airborne, sublimation losses are reduced. *Sturm et al.* [2001b] showed that the greatest snow depth occurred downwind of the maximum shrub height along a 100 m transect where canopy height first increased from 0.5 m to 1.2 m and then declined to 0.25 m. *Pomeroy et al.* [2006] measured snowfall and snow accumulation in shrub and sparse tundra over a period of 7 a in the Yukon Territory. They found that the maximum snow accumulation in the shrub tundra averaged nearly 2.5 times that in the sparse tundra even while the snowfall in both areas was similar. These results show that increasing the area covered by shrubs in arctic Alaska would increase the mass of snow retained through the winter.

[5] The significance of increased shrubs in the Arctic was also shown by *Liston et al.* [2002]. They used a blowing snow model along with a simple surface energy balance model to show that increased shrubs over a 4 km^2 domain in

[1]Cooperative Institute for Research in the Environmental Sciences, University of Colorado, Boulder, Colorado, USA.
[2]Cooperative Institute for Research in the Atmosphere, Colorado State University, Fort Collins, Colorado, USA.

0148-0227/07/2006JG000297$09.00

arctic Alaska led to significant decreases (68%) in sublimation losses and therefore increases in end-of-winter snow depth. The greater amount of snow retained through the winter then leads to larger runoff magnitudes during the melt period.

[6] Although the effects of increased shrubs on snow distributions and properties was examined through both observational and modeling studies, very little has been done to investigate the effects on the Arctic atmosphere during the spring melt season. *Liston et al.* [2002] did not utilize an atmospheric model and so nothing could be determined about the influence of increased shrubs on air temperature and precipitation. Also, the simple surface energy budget model used was not able to represent the shading, longwave, and sensible heat emission effects of the shrubs during the melt season. Emission of longwave radiation and turbulent sensible heat by the shrubs during the spring could cause the snow to melt more rapidly even though there is more snow water equivalent (SWE), which would have a strong impact on the surface energy budget. The model used in the study described in this paper has the capability to simulate the feedback of the shrubs to the atmosphere. In addition, the model can simulate shading, longwave, and sensible heat emission effects of the shrubs during the melt season.

[7] There has been a considerable amount of research illustrating how snow can significantly reduce daytime temperatures by as much as 10°C on timescales of days to months [*Namias*, 1985; *Cohen and Rind*, 1991; *Baker et al.*, 1992; *Leathers and Robinson*, 1993; *Ellis and Leathers*, 1998]. Snow cover reduces daytime temperatures by increasing the net surface albedo and reducing the maximum attainable surface temperature. First of all, the higher surface albedo reduces the amount of incoming solar radiation that can be absorbed, meaning less energy will be available to heat the surface and nearby air. Second, the temperature of the snow is limited to 0°C or less. Once the snow temperature reaches 0°C, the remaining energy can only be used for melting. These two effects combine to produce a surface that is significantly cooler than its snow-free counterpart under the same ambient conditions.

[8] *Strack et al.* [2003] found, using the Colorado State University Regional Atmospheric Modeling System version 4.3 (CSU-RAMS 4.3.0), that daytime near-surface air temperatures over snow were increased when the quantity of vegetation protruding through ephemeral snow cover in the Texas Panhandle was increased. The fractional area of shrubs in that study decreased linearly from 0.5 to 0 as the snow depth approached the top of the shrubs. The authors of that study found that protruding vegetation increased sensible heat fluxes as much as 80 W m^{-2} and daytime temperatures by as much as 6°C. In addition, they found that afternoon boundary layer height increased as much as 200–300 m.

[9] *Sturm et al.* [2005] measured incoming and reflected solar radiation over shrubs of various heights during two winter seasons in western Alaska. Their observations suggest shrubs protruding through a tundra snowpack reduce the net surface albedo by as much as 30% and can increase absorbed solar radiation up to 75% during the snow season. They mention that this is approximately two thirds as strong as the increase that would be associated with tundra to forest transition.

[10] *Pomeroy et al.* [2006] measured radiative fluxes both above and below the shrub canopy and turbulent heat fluxes above the canopy at several shrub tundra sites in the Yukon Territory during the 2003 spring melt season. They found the shrubs increased the amount of sensible heat flux to the atmosphere and increased the net longwave radiation at the snow surface. In addition, they found the shrubs increased snowmelt rates even though the solar radiation reaching the snow surface was reduced. Over a 7 a period the duration of the spring melt season was about 7 d longer on average in the shrub tundra sites.

2. Methods

[11] In order to examine the effects of the shrubs and soot, two modeling systems were used in tandem to simulate the accumulation and melt of snow during the winter and spring, as well as atmospheric temperatures during the spring melt period, for three fall-winter-spring seasons in the Kuparuk Basin of Alaska. The blowing snow model, SnowTran-3D [*Liston and Sturm*, 1998a], was utilized to simulate the accumulation period (September–April). The spring melt period (May–June) was simulated using the CSU-RAMS version 4.4 [*Cotton et al.*, 2003], equipped with a modified snowpack model.

[12] The snow model is contained in the Land Ecosystem-Atmosphere Exchange Feedback version 2 (LEAF-2) [*Walko et al.*, 2000] land surface model of RAMS. Four basic components, canopy air, vegetation, temporary surface water (snow), and soil, comprise LEAF-2. The canopy air is defined to be the air below the defined vegetation height when vegetation is present. When no vegetation is present, the "canopy" air is defined to be the air in the laminar sublayer. At each time step, energy and moisture balances are carried out for each of these components. The turbulent sensible and latent heat fluxes between vegetation and canopy air are proportional to the fraction of total leaf area index (LAI) that protrudes above the snowpack. Similarly, the emission and absorption of longwave radiation and the absorption of shortwave radiation are proportional to the portion of the vegetation fraction that protrudes above the snow. The vegetation fraction is considered to be the fraction of the ground/snow that is obscured by vegetation when viewed directly from above. This protruding LAI fraction and vegetation fraction decreases linearly to zero as the snow depth approaches the vegetation height. LEAF-2 in its present state can not accurately produce sensible heat fluxes from vegetation that is completely bare of leaves, since it is based on LAI. In order to correct this deficiency, the sensible heat flux from the shrubs was modeled as being equal to the net radiation absorbed by the branches, as in the work of *Otterman et al.* [1993]. This assumes that the heat capacity of the shrubs is very small and that there is no significant cooling due to the latent heat of evaporation. Cooling of the shrubs by latent heat of evaporation was negligible for most of this simulation, since they were mostly dormant during the snow melt season. This is the same method used by *Strack et al.* [2003].

[13] Six major changes have been made to the snow component of the RAMS. These changes include snow

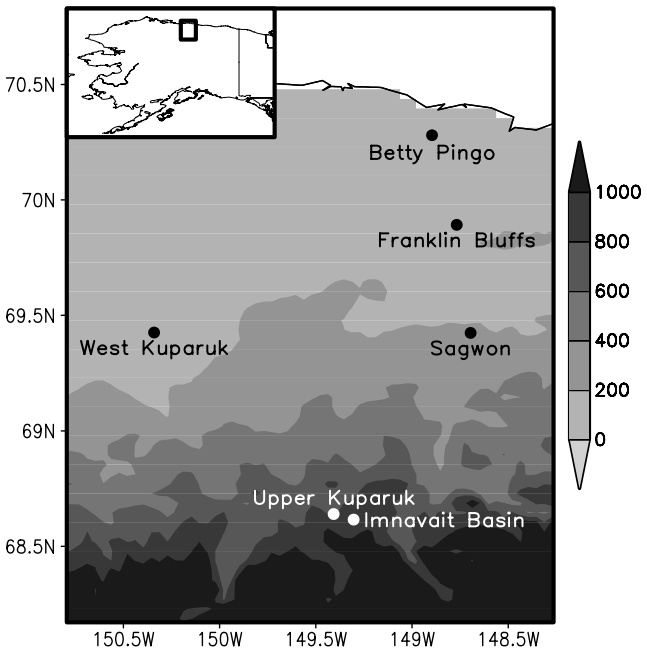

Figure 1. Map showing the locations of the Kuparuk meteorological stations (solid circles). Topography is shown in 200 m intervals.

depth prediction, prediction of the falling snow density, addition of a new snowpack compression rate, a new age-based snow albedo formulation, addition of a subgrid-scale snow depth distribution model [*Liston*, 2004], and prediction of the snow skin temperature. The modified snow model is described in more detail by *Strack et al.* [2004].

2.1. Atmospheric Initialization

[14] Three nested grids were used in this study. The outer coarsest grid covered most of Alaska and had horizontal grid intervals of 72 km. The second grid covered a large part of north central Alaska and had horizontal intervals of 18 km, while the innermost grid was centered on the Kuparuk Basin with horizontal grid intervals of 4.5 km. The approximate area covered by the fine grid is shown in Figure 1. On the two outer grids, vertical grid intervals ranged from 300 m near the surface to 1000 m above the 12 km level. Vertical grid intervals on the fine grid ranged from 33 m near the surface to 1000 m above the 12 km level. The two coarse grids had a total of 27 levels reaching an altitude of about 18 km. The fine grid had 63 levels which also extended to about 18 km.

[15] The model was initialized at 1200 UTC 1 May for all three years, 1995, 1996, and 1997, with the NCAR-NCEP reanalysis derived temperature, specific humidity, geopotential height, and winds [*Kalnay et al.*, 1996]. Although the reanalysis is relatively coarse in spatial resolution (210 km), it is adequate for initializing the upper layers of the model. Surface observations in the Kuparuk Basin, provided by the University of Alaska Fairbanks Water and Environmental Research Center (WERC), were also incorporated into the atmospheric initialization fields to improve the initial representation of the boundary layer. The simulations were all terminated in late June of each year after most of the significant snow had melted in the fine domain. The Smagorinsky [*Smagorinsk*, 1963] and Mellor-Yamada [*Mellor and Yamada*, 1982] turbulence schemes were used for horizontal and vertical diffusion, respectively. The Smagorinsky scheme calculates the horizontal diffusion coefficients as the product of the local horizontal deformation rate and a length scale proportional to the horizontal grid increment. The Mellor-Yamada scheme uses turbulent kinetic energy simulated from the model's prognostic velocity components to calculate the vertical diffusion. Both shortwave and longwave radiation were parameterized using the Chen and Cotton [*Chen and Cotton*, 1983] routine. The Chen and Cotton routine uses the full radiative transfer equation to simulate longwave radiation and a three-band scheme for shortwave radiation. Both schemes account for condensate in the atmosphere but do not distinguish between cloud water, rain, or ice. The boundaries of the outermost grid were nudged toward the NCAR-NCEP reanalysis every 6 h during the course of the simulation.

2.2. Land-Cover Specification

[16] For all simulations, the 1 km resolution Advanced Very High Resolution Radiometer (AVHRR) derived Olson Global Ecosystem (OGE) land-cover data [*Olson*, 1994a, 1994b] was used to specify the land cover in regions outside of the North Slope of Alaska. The land cover for the North Slope was specified from the 100 m resolution Northern Alaska-Multi-Spectral Scanner (NA-MSS) data set [*Muller et al.*, 1999]. For the shrub-enhanced simulation, the moist and moist/wet tundra land cover types were considered suitable for invasion by shrubs and were therefore replaced with the shrub category. The polluted snow simulation used the same vegetation as the control simulation.

[17] In RAMS 4.4, LEAF-2 cross references all vegetation types to one of 18 Biosphere-Atmosphere Transfer Scheme (BATS) [*Dickinson et al.*, 1986] categories for which physical parameters have been defined. The vegetation physical parameters used by LEAF-2 are albedo, LAI, vegetation fraction, emissivity, roughness length, displacement height, and root depth. In these simulations most of the North Slope was cross-referenced to the deciduous shrub and tundra BATS categories. The displacement heights of tundra and shrubs were adjusted from their BATS values to correspond to canopy heights given by *Liston and Sturm* [2002]. The resulting canopy heights for shrubs and tundra were 0.5 m and 0.1 m, respectively. In addition, the LAI of shrubs was adjusted to zero since they are bare during most of the simulation period. The vegetation fraction of the shrubs was also adjusted to 0.7 due to lack of leaves. Finally, tundra vegetation fraction was adjusted to 0.9 to account for the thick organic mat which covers most of the soil. The default BATS values were used for all the other vegetation parameters. In the shrub enhanced simulation the shrub canopy height was increased to 0.75 m and all other vegetation parameters remained the same as in the control. The vegetation parameters in the polluted snow simulation were the same as those in the control run.

2.3. Snow-Cover Initialization

[18] The initial SWE on the fine grid was derived by running the blowing snow model SnowTran-3D from 1 September to 30 April of each year as described by *Liston and Sturm* [2002]. At regional scales the end-of-winter SWE in the Arctic is closely approximated by the difference between the total winter precipitation and the loss due to sublimation. *Liston and Sturm* [2002] used this relationship to estimate the total winter precipitation for each of the years simulated in this study, namely 1995, 1996, and 1997. They iterated the model starting with a first guess for total winter precipitation equal to the observed 200 km north-south transect of end-of-winter SWE. The total precipitation was adjusted with each iteration until the average end-of-winter SWE at each latitude in the model was equal to the observed value. This SWE field was used for initialization of the fine grid in the control runs. The SWE on the fine grid for the enhanced shrub simulation was obtained by replacing the moist/wet tundra and moist tundra with shrubs on the SnowTran-3D domain and rerunning with the precipitation fields obtained above. In addition, since the shrubs were assumed to have become larger in the shrub enhanced simulation their height, and thus snow-holding capacity, was increased by 50%. Following *Liston and Sturm* [2002] the snow-holding capacity was assumed to be equal to 80% of the maximum vegetation height. The initial SWE for the polluted snow simulation was the same as for the control.

[19] The SWE for portions of the coarse grids located outside the fine grid region was initialized with the April values of the Global Monthly EASE-Grid Snow Water Equivalent Climatology data set [*Armstrong et al.*, 2005]. This data set is a 25 km grid of Scanning Multichannel Microwave Radiometer (SMMR) and selected Special Sensor Microwave/Imagers (SSM/I) derived monthly mean SWE values. This data set has a number of known errors including overestimation in regions of strong depth hoar formation such as the North Slope; however, it is the best available for the region outside of the fine grid during the years simulated.

[20] Snow densities for the fine grid region were initialized from values observed by *König and Sturm* [1998] for each year. Each grid cell on the outer grids was assigned one of six snow cover classes from the Global Seasonal Snow Classification System [*Liston and Sturm*, 1998b]. Snow in these cells was then assigned a typical density [*Liston et al.*, 1999] based on its class. Coefficients of variation for use with the Subgrid SNOW Distribution (SSNOWD) model [*Liston*, 2004] were also assigned to each cell based on these classes.

[21] Snow albedo was modeled using the equations *Douville et al.* [1995] developed from *Baker et al.* [1990] and *Verseghy* [1991], where the albedo decreases with time since last snowfall from a fresh snow maximum of 0.85 to a minimum value of 0.5. In this application the reduction in albedo with age has been decreased by 50% and the minimum value increased to 0.55 to better match the observed snow albedo at the Kuparuk meteorological stations. Snow albedo was initialized based on time since last snowfall, as determined from the precipitation estimates generated by the SnowTran-3D simulations. In the polluted snow simulation the fresh snow albedo was set to 0.75 and the minimum for old snow was set to 0.45. The decrease of 0.1 in this case represents the effect of soot contamination. The value of 0.1 was chosen based on data presented by *Hansen and Nazarenko* [2004].

2.4. Soil Temperature and Moisture Initialization

[22] There were eight soil layers extending down to 3 m depth. The soil layer thickness ranged from 0.05 m near the surface to 1 m at the deepest level. The soil types were specified from the Food and Agriculture Organization of the United Nations (FAO) data set [*Food and Agriculture Organization*, 1997]. Soil temperature and moisture were specified from the 32 km National Center for Environmental Prediction North American Regional Reanalysis (NCEP-NARR) [*Mesinger et al.*, 2006]. Although it is well known that liquid water can exist in soil below 0°C, the soil moisture was defined as all ice when the soil temperature was 0°C or less due to a lack of suitable ice/liquid fraction data. This assumption had little effect on the simulation results since the soil is beneath deep snow which melts from the top down due to solar radiation.

3. Results

3.1. Control Run

[23] RAMS has previously been proven a robust high quality modeling system [*Cotton et al.*, 2003]. The purpose of the control runs is to further prove the model's ability. In this section a discussion of the results of the control run is given. Observed values of snow water equivalent at Imnavait Basin and Betty Pingo, AK are compared with those simulated by the model; see Figure 1 for station locations. In addition, observed 3 m air temperatures at the Imnavait Basin, West Kuparuk, Upper Kuparuk, Franklin Bluffs, Sagwon, and Betty Pingo meteorological stations are compared with simulated values. Finally, the observed incoming shortwave and longwave radiation, albedo, and net radiation at these stations are also compared with the model output. The data from these stations was obtained through the WERC Web site [*Kane and Hinzman*, 2005]. These comparisons show how well the model can simulate the present day conditions in the Kuparuk Basin.

3.1.1. Snow Water Equivalent

[24] The observed evolution of snow water equivalent at the Imnavait research basin and Betty Pingo meteorological station are shown by the black circles in Figure 2. Imnavait Basin is an approximately 2.2 km^2 research watershed centered near 68.6°N and 149.3°W [*Kane et al.*, 1997]. Betty Pingo is located on the Arctic coastal plain at the northern end of the Kuparuk Basin. Every few days during the melt period, 50 snow depth and 5 snow density measurements were made at each of six sites along a transect across the Imnavait watershed. Four of the sites were located on the west facing slope of the basin, one was located on the valley bottom, and one was located on the east-facing slope. The west-facing slope represents about 78% of the basin while the east-facing slope and valley bottom represent 17 and 5% of the basin, respectively. The values shown in Figure 2 are area-weighted averages of the west- and east-facing slopes and the valley bottom. Every few days during the melt period, 50 snow depth and 10 snow density measurements were also made at each of three

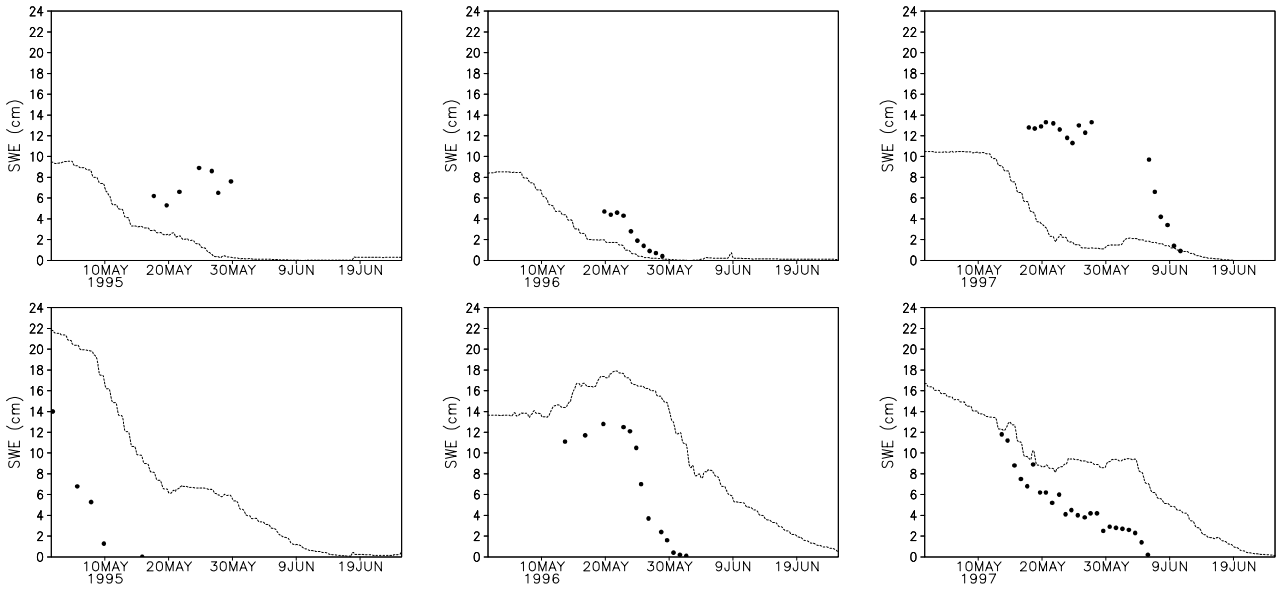

Figure 2. Observed and simulated SWE for (top) Betty Pingo and (bottom) Imnavait Basin. Solid circles represent observations; black dashed line represents modeled values.

sites located within a 0.08 km^2 watershed [*Mendez et al.*, 1998] centered near the Betty Pingo station.

[25] The black dashed lines in Figure 2 show the snow water equivalent evolution as simulated at the model grid cells containing Imnavait Basin and Betty Pingo. In all years the simulated snow melted too quickly at the Betty Pingo site. This could be due to excessively high incoming solar radiation, discussed in the next section, in the model. In contrast, the simulated snow at the Imnavait basin location persisted much longer than the observed values. However, it should be noted that the simulated snow depths are for the grid cell containing the observation stations. The values shown for Imnavait basin represent an area of 2.2 km^2 while the grid cell covers 20.25 km^2. It is possible that the snow remaining in the grid cell is located outside of the area of measurements. The grid cell containing Imnavait Basin was 35, 28, and 40% snow free at the time the observed snow in the watershed was gone in 1995, 1996, and 1997, respectively. A very small amount of snow persists until the end of the simulation in 1996 and 1997, but it covers less than 10% of the cell and represents a few deep drifts.

3.1.2. Radiative Fluxes and Air Temperature

[26] The simulated albedo started around 0.85 for all the stations, except Betty Pingo which started at 0.72, and fell gradually to around 0.2 as the snow ablated. The simulated albedo generally decreased more slowly than the observed values during the melt period. This could be due to the fact that the meteorological towers see a smaller and more homogeneous region than the 4.5 km grid cells in the model. The snow will disappear from the footprint of the tower in a much shorter period of time than over the large grid cell which likely contains more heterogeneity in snow cover. The observed snow-free albedo was about 0.05 and 0.1 lower than the simulated values at the Upper Kuparuk and West Kuparuk stations, respectively. The observed snow-covered albedo appeared to be 0.1 to 0.2 higher than the modeled values at the Upper Kuparuk station. Observed snow-covered albedo at the other stations was similar to those in the model. The diurnal pattern in the simulated albedo at Betty Pingo, Franklin Bluffs, and West Kuparuk was due to the presence of lakes and their associated zenith angle-dependent albedo.

[27] At the stations where observations were available the simulated solar radiation often varied widely from the observed, often either over or underestimating by 500 W m^{-2} or more. The model underestimated the downward longwave radiation at Imnavait Basin and the Upper Kuparuk station, often by 50 W m^{-2} or more. The model tended to overestimate the downwelling longwave radiation at West Kuparuk during the first part of the simulation and alternated between overestimating and underestimating during the latter part of the simulation.

[28] The frequently underestimated downward longwave radiation in the model may play a role in the delayed snow melt. Snow is a near perfect absorber of longwave radiation, and thus its rate of melt is very sensitive to changes in this quantity. The effects of the overestimation in incoming solar radiation mentioned earlier could be more than offset by the reduced longwave radiative flux, leading to the overall sluggish snowmelt in these simulations.

[29] The model tended to overestimate the net radiation during the daytime at Betty Pingo, especially during the first part of the simulation. On the other hand, the net radiation was often too small during the daytime at Imnavait Basin and Sagwon. In addition, the simulated upward radiation appeared to be too large during the nighttime at these two stations. The modeled net radiation at West Kuparuk and the Upper Kuparuk station appeared to be too large during most of the simulation. Although the magnitudes were off the model did capture some of the synoptic variability, such as the observed decrease in early May at Imnavait Basin and West Kuparuk.

Table 1. Statistical Comparison of Control Run to Observations

Parameter	3-m Air Temperature, °C	Shortwave Radiation, W m^{-2}	Downward Longwave Radiation, W m^{-2}	Net Albedo	Net Radiation, W m^{-2}	Snowmelt Rate, cm h^{-1}
E	5.8	149	51	0.39	87	0.095
EU	5.2	149	51	0.38	87	0.092
σ_{obs}	6.5	214	40	0.36	94	0.093
σ	5.7	247	60	0.19	102	0.044
N	5893	4782	4612	6157	4983	70

[30] The model was able to capture the synoptic-scale variations in temperature fairly well at all stations. However, the temperatures were consistently too low at Imnavait Basin, West Kuparuk, and the Upper Kuparuk station. The temperatures tended to be closer to the observations or slightly warmer at the northern stations. Part of the cool bias at the southern stations was likely due to the more persistent snow at these locations in the model. When averaged over all years, the model averaged 2.5°C cooler than the observations during the month of May.

3.1.3. Statistical Comparison of Control Run to Observations

[31] The root mean square error (E), root mean square error with bias removed (EU), and the standard deviations of the predictions (σ) and observations (σ_{obs}) for the quantities mentioned above for all three years simulated are listed in Table 1. The parameter N in Table 1 represents the number of comparisons for each parameter. All of these statistics were calculated using equation (12.20) of *Pielke* [2002] developed by *Keyser and Anthes* [1977]. According to *Pielke* [2002], a model demonstrates skill when $\sigma \approx \sigma_{obs}$, $E < \sigma_{obs}$, and $EU < \sigma_{obs.}$ This method has been applied in many modeling studies including *Pielke and Mahrer* [1978], *Segal and Pielke* [1981], and *Shaw et al.* [1997]. This study was most interested in the predominately snow-covered period, and so the following statistics were compiled only for the month of May when snow cover is most prominent.

[32] Table 1 shows that the model simulated the 3 m air temperatures well, with a root mean square error of 5.8°C and σ_{obs} = 6.5°C. These results are comparable to the root mean square error in near-surface air temperatures in a snow modeling study by *Narapusetty and Mölders* [2005]. They ran test simulations with the Hydro-Thermodynamic Soil-Vegetation Scheme (HTSVS) coupled to the Pennsylvania State University-National Center for Atmospheric Research (NCAR) Mesoscale Meteorological Model (MM5) and calculated root mean square errors around 11°C near the end of the 120 h simulations. Even though their simulations are much shorter than those described in this paper, the results still suggest the E value of 5.8°C are reasonable for a mesoscale model such as RAMS. Since the E for modeled quantities tends to increase with the length of a simulation the average value of 5.8°C for the entire 2 month simulation is respectable, considering the E surpasses 10°C after just 120 h of simulation in the MM5 study.

[33] A review of the rest of Table 1 shows that the model skillfully simulated net radiation as well as incoming solar radiation. However, the results for the net surface albedo, downward longwave radiation, and snowmelt rates suggest lower skill levels for the model in predicting these quantities. Even though many of the errors appear large the primary interest in this study is the change a perturbation will have on the model response. Some of the same sources of error in the control, such as the magnitudes of downward longwave and shortwave radiation, are likely also present in the perturbation runs and cancel out when the differences are calculated.

3.2. Perturbation Simulations

[34] On the basis of the results shown in the previous section, the modeling system is believed to have the skill and robustness necessary for examining the effects of increasing shrubs or soot on the tundra snowpack and atmosphere through a set of perturbation simulations. In this section the results of the perturbation simulations are compared with those of the control. The two perturbation simulations were the enhanced shrub and polluted snow cases. In the enhanced shrub simulation all the moist and moist/wet tundra categories on the North Slope were replaced with shrubs. The wet tundra category was not replaced with shrubs, since it is not considered suitable for shrub establishment. It is also possible that some of the moist/wet tundra is not suitable, but a complete invasion of this category was allowed in order to get a worst-case scenario for shrub expansion. Replacing the moist and moist/wet tundra changed the total area of shrub coverage from 2276 km^2 to 9522 km^2 in the fine grid. In addition, the average shrub height was increased 50%. As a result, the SWE was greater over much of the domain in the enhanced shrub simulation. The same general patterns held for the other two years. In the polluted snow simulation the initial snow albedo was decreased by 0.1. In all other respects the perturbation runs were identical to the control, and therefore any observed differences in the results can be attributed to the perturbations themselves.

[35] Figure 3 shows the time evolution of domain average SWE in each year for all three simulations. Domain average in this discussion refers to the average over the fine grid. In each year the enhanced shrub simulation initially had more snow than the control. This is to be expected since the shrubs reduce blowing snow losses during the winter months. The melt rate in the enhanced shrub simulation proceeded more rapidly than in control, especially during the onset of melt, and the snow melted off 11 d earlier. This is due to the warming of the air and emission of longwave radiation by the protruding shrubs. The domain-averaged vegetation height above the snow surface is shown in Figure 4. The melt rate in the shrub simulation began to slow and approach that of the control simulation toward the end of the melt period. This is likely due to the shading effect of the shrubs becoming stronger as the snowpack decreased in depth.

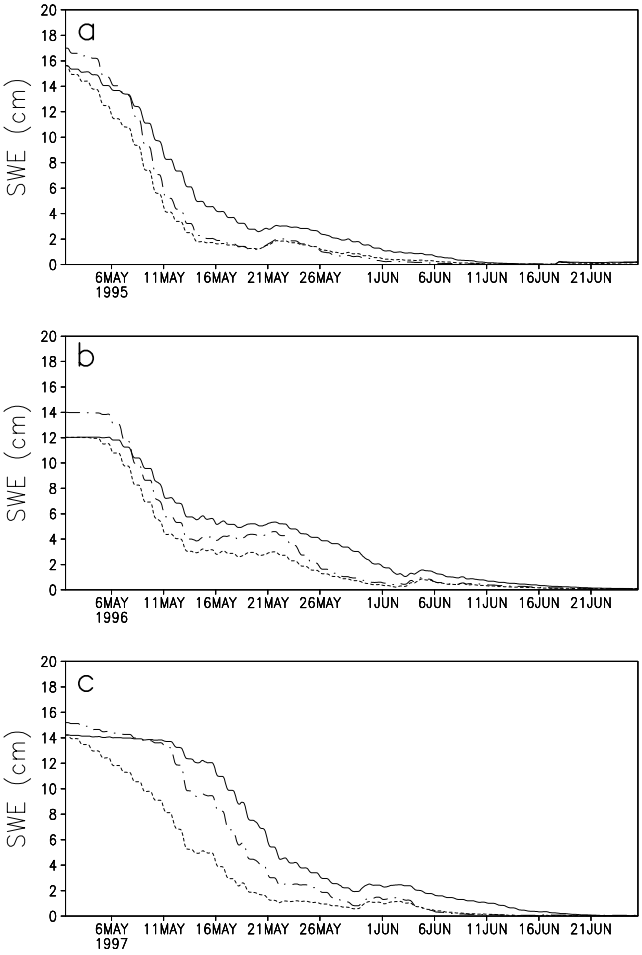

Figure 3. Domain-averaged SWE for the control (solid), shrub-enhanced (dash-dotted), and polluted snow (dashed) runs for (a) 1995, (b) 1996, and (c) 1997.

[36] The melt rate in the polluted snow case was also faster than the control, but not as fast as in the shrubs. However, since the initial snow depth was the same as in the control the differences in depth during the melt period are greatest in this simulation. The polluted snow also melted off about 5 d faster than in the control case.

[37] The net radiation gradually increased toward the end of the simulations as the albedo decreased and incoming solar radiation increased. As expected, the net radiation was greater in both perturbation simulations during the snow-covered period due to the lower net surface albedo. The relatively dark shrubs protruding through the snowpack lower the net surface albedo significantly allowing for more solar radiation to be absorbed during the day. The extra energy is then transferred to the atmosphere through sensible heating. The polluted snow has a lower albedo and hence absorbs more solar radiation regardless of the amount of protruding vegetation. Figure 5 shows a time series of the net radiation for a 3 d period during the peak melt period. The net radiation averaged 28 and 23 W m^{-2} higher during the month of May in the shrub and polluted snow simulations, respectively.

[38] The sensible heat flux started off small or negative with a weak diurnal cycle in all simulations. As more snow-free areas appeared daytime sensible heat flux grew larger in all the simulations. The sensible heat flux in the shrub simulation was much higher, often by 50 W m^{-2}, during the snow-covered period of the simulation than in the control. This is due to the relatively warm shrubs protruding through the snowpack. As the snow melted away, the sensible heat flux in the shrub simulation became smaller than in the control. This was due to the greater amount of exposed soil in the modeled shrubs. The energy absorbed by the soil was used to melt the ice and therefore was not available to raise the surface temperature. The tundra vegetation covered more of the ground and cut off the cold soil from the overlying air. Since the tundra vegetation had a much lower heat capacity, it could easily warm above ambient air temperature. However, it is not certain if this effect is seen in reality since in most cases the tundra organic mat lies beneath shrubs. In addition, observations by *Chapin et al.* [2000] do not suggest any strong depression in sensible heat fluxes over shrub tundra. LEAF-2 can not simulate such a double canopy in its present state, so there was no choice

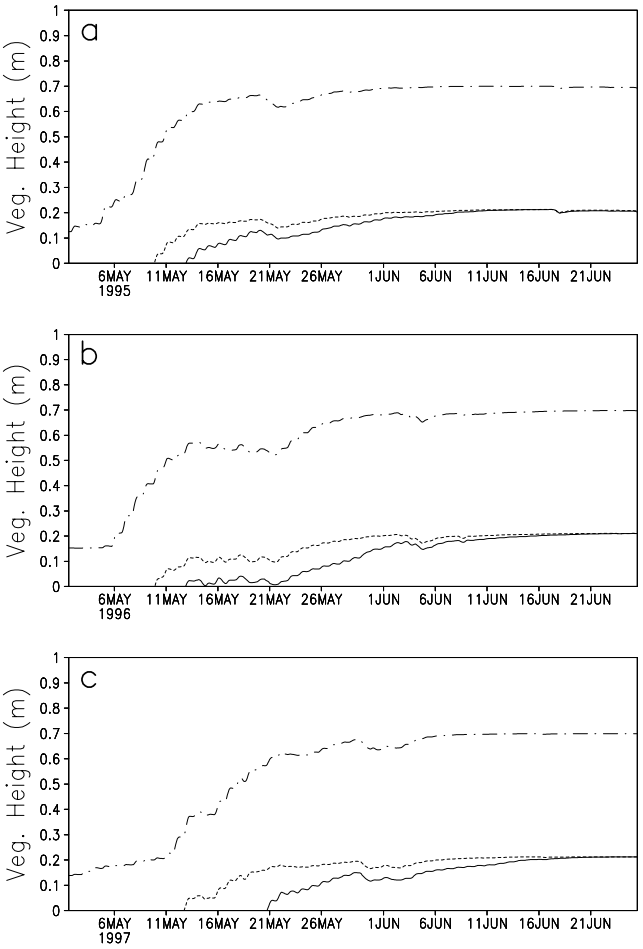

Figure 4. Domain-averaged vegetation height above snow for the control (solid), shrub-enhanced (dash-dotted), and polluted snow (dashed) runs for (a) 1995, (b) 1996, and (c) 1997.

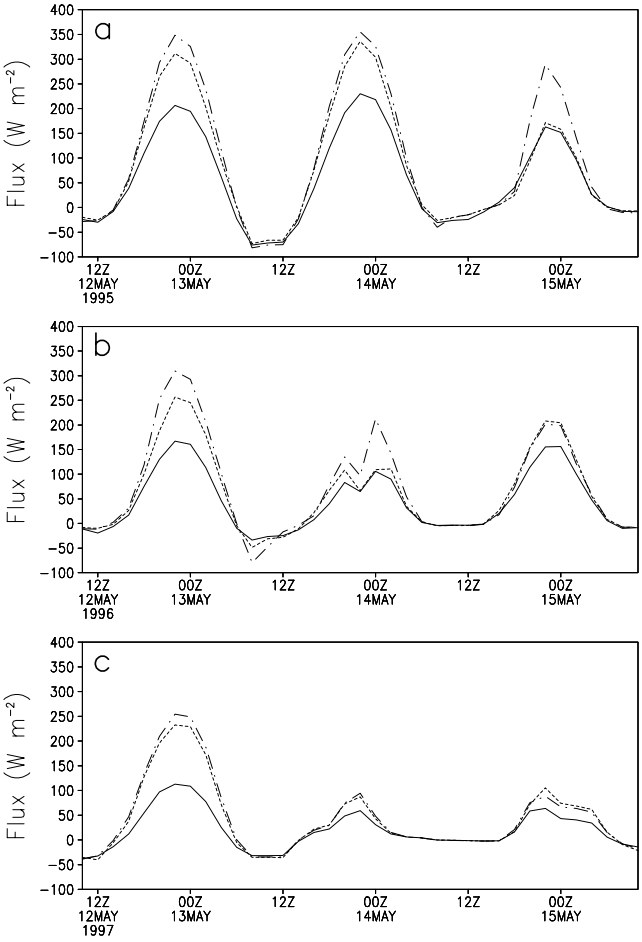

Figure 5. Domain-averaged net radiation for the control (solid), shrub-enhanced (dash-dotted), and polluted snow (dashed) runs for (a) 1995, (b) 1996, and (c) 1997.

but to have bare soil underlying the shrubs. The sensible heat flux averaged 17 W m^{-2} higher in the shrub run during May.

[39] The sensible heat flux in the polluted snow simulation was closer to that in the control run. This is expected since the snow is limited to 0°C regardless of how low the albedo is. The main differences occur when the snow temperature is well below freezing and solar radiation is strong. In these cases the polluted snow can warm to greater temperatures than clean snow and produce a larger sensible heat flux. The sensible heat flux in the later part of the simulation was slightly greater in the polluted snow case. This is likely due to the slightly warmer soil from the earlier snow melt. The sensible heat flux averaged 2 W m^{-2} higher in the polluted snow run during the month of May. Figure 6 shows an example of domain-averaged surface sensible heat flux for the three simulations.

[40] In all the simulations the latent heat flux peaked during the snow melt period. The latent heat flux started off small and gradually increased as the amount of liquid water increased during the melt period. The latent heat flux tapered off late in the period as the amount of surface moisture declined. This version of the model does not include transpiration, and it should be noted that some of this decline in latent heat flux might be offset in nature by increasing transpiration by vegetation. Higher peak values occurred in the enhanced shrub case due to the warmer air. Slightly higher peak values occurred in the polluted snow case when the polluted snow was able to warm the nearby air more than clean snow. Time series of the latent heat flux for a 3 d period are shown in Figure 7. On average, during the entire month of May, the latent heat flux was 10 and 2 W m^{-2} higher in the shrub and polluted snow cases, respectively.

[41] The pattern of temperature (see Figure 8) closely followed the pattern of sensible heat fluxes discussed earlier. The largest differences occurred in the shrub enhanced simulation. The days in Figure 8 that show little difference between runs are characterized by low incoming solar radiation due to cloud cover. The effects of protruding vegetation are strongest in clear sky conditions where solar radiation is strong. During the month of May, the shrub enhanced simulation averaged 2.2°C warmer than the control. The temperatures in the polluted snow run averaged only 1.0°C warmer. During the month of May the planetary boundary layer height was generally less than 1000 m but occasionally peaked around 1500 m. The deepest boundary layer occurred in the shrub enhanced simulation and is a result of the greater sensible heat flux generated by the

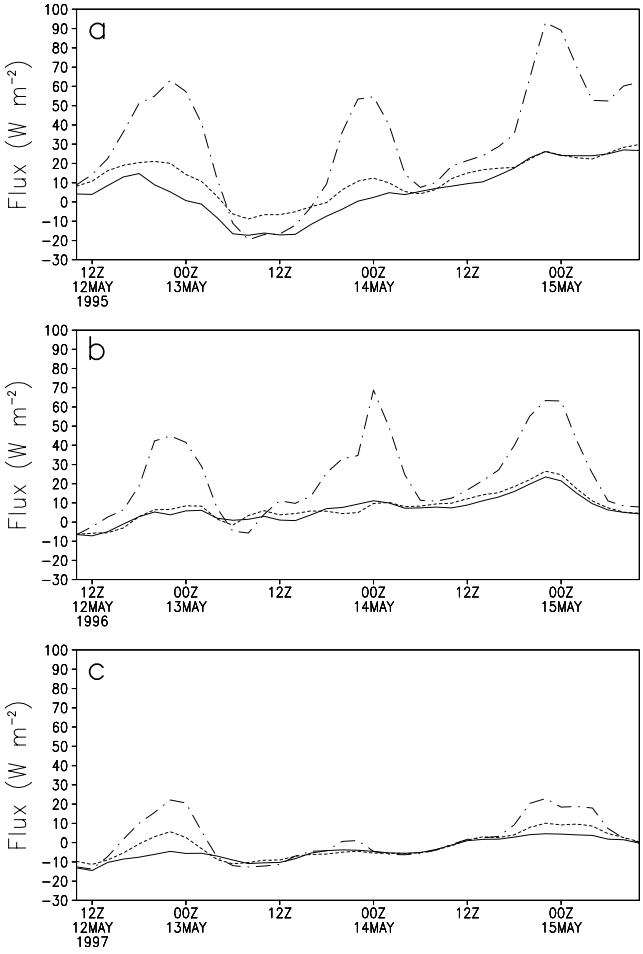

Figure 6. Domain-averaged sensible heat flux for the control (solid), shrub-enhanced (dash-dotted), and polluted snow (dashed) runs for (a) 1995, (b) 1996, and (c) 1997.

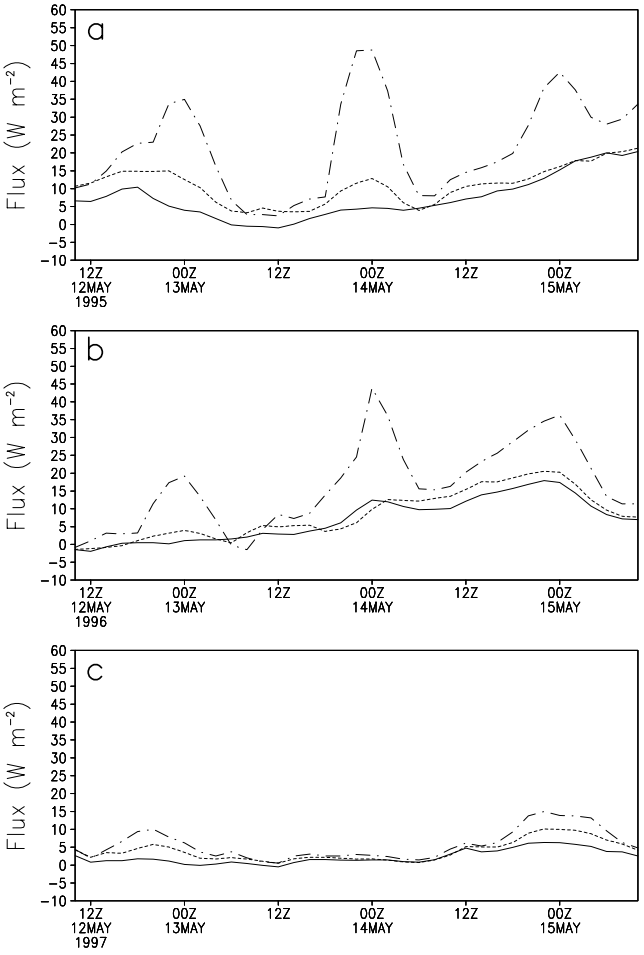

Figure 7. Domain-averaged latent heat flux for the control (solid), shrub-enhanced (dash-dotted), and polluted snow (dashed) runs for (a) 1995, (b) 1996, and (c) 1997.

protruding shrubs. The planetary boundary layer depth in the shrub enhanced simulation often grew several hundred meters deeper than in the control during the month of May, and on average was 108 m deeper when snow was present. The difference between the polluted snow case and the control run was generally smaller, averaging 25 m deeper in the polluted snow run when the snow was present. Figure 9 shows a close up view of the boundary layer height time series for a 3 d period in May.

3.3. Statistical Comparison of the Perturbation Runs to the Control Run

[42] In order to determine the significance of these perturbations, paired t-tests were used to construct confidence intervals for the mean differences in the variables mentioned in the previous section. One should note the potential exists for spatial autocorrelation in these data grids. The t-tests, however, still provide a useful assessment of the significance of the means. A similar use of t-tests was made by *Eastman et al.* [2001] when comparing the influence of vegetation changes on grids of model response variables.

[43] Table 2 displays the 99.9% confidence intervals for the mean differences between 3 m air temperature, sensible heat flux, latent heat flux, net radiation, snowmelt rate, planetary boundary layer height, and snow-free date. These values were determined by calculating the mean difference over all grid points for each time step during May of each year examined. There were 695,520 comparisons for each response variable. The confidence intervals show that all the differences were significant at the 99.9% confidence level except for the snow melt rate in the soot simulation. The 99.9% confidence interval for the snow melt rate in the soot case includes zero and so is not significantly different from the rate in the control run. However, this analysis shows that most of the response variables of interest in the perturbation runs are significantly different at a very high level of confidence. Furthermore, these results strengthen the theory that shrub expansion and soot deposition can have a significant impact on near-surface weather and climate during the snowmelt period and should be accounted for in long-term simulations of global climate.

4. Discussion

[44] Past research has shown that shrub encroachment in the Arctic increases the amount of snow retained through the winter by reducing the amount lost through sublimation

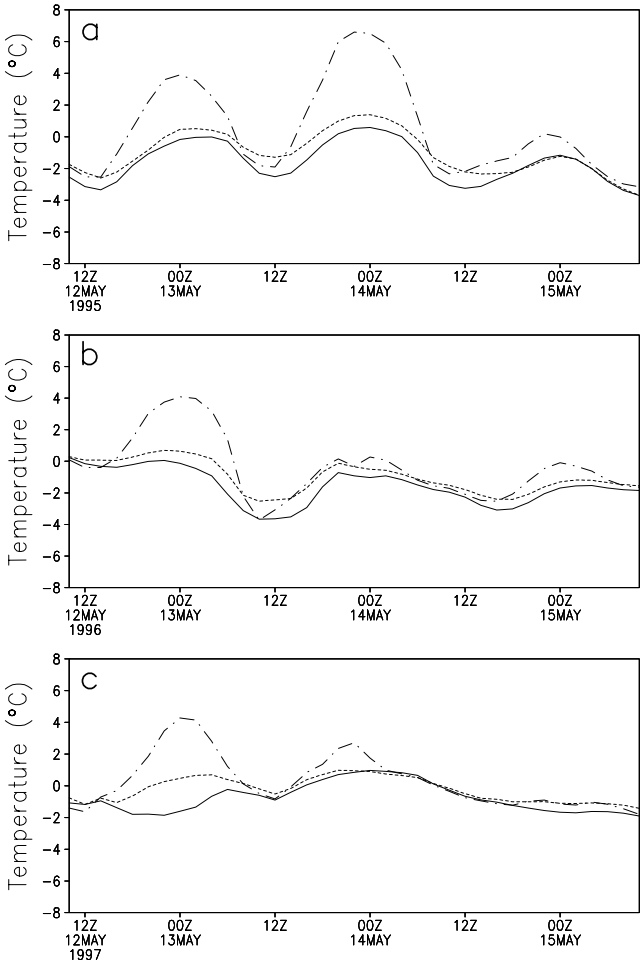

Figure 8. Domain-averaged 3 m air temperature for the control (solid), shrub-enhanced (dash-dotted), and polluted snow (dashed) runs for (a) 1995, (b) 1996, and (c) 1997.

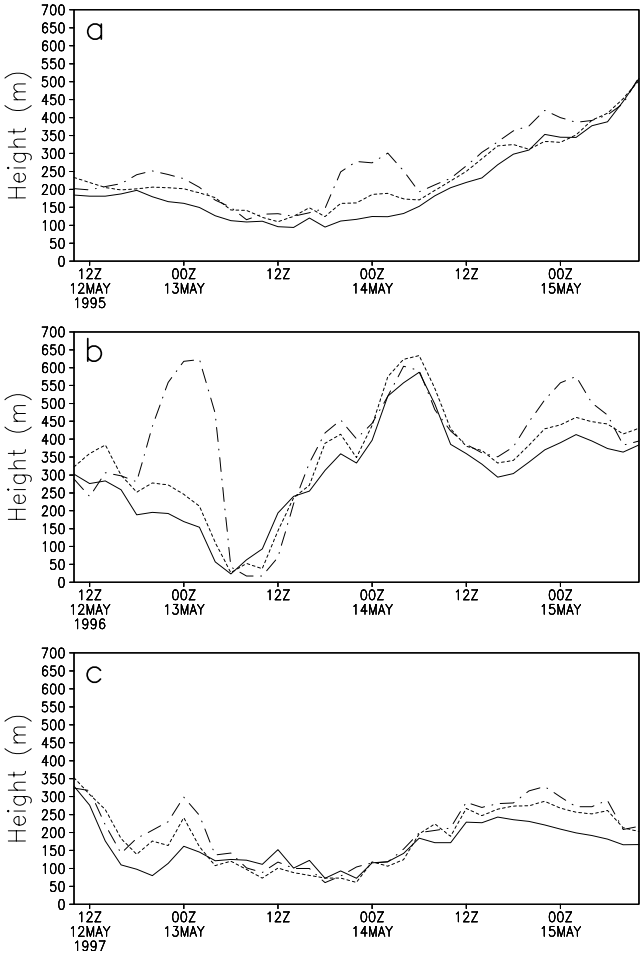

Figure 9. Domain-averaged planetary boundary layer height for the control (solid), shrub-enhanced (dash-dotted), and polluted snow (dashed) runs for (a) 1995, (b) 1996, and (c) 1997.

of blowing snow. The shrubs break the force of the wind, making it more difficult for snow particles to become airborne. As a result, less snow particle surface area is exposed to the air and the loss due to sublimation is reduced. The net result is a deeper end-of-winter snowpack given the same amount of overwinter precipitation.

[45] Although shrub invasion leads to a deeper end-of-winter snowpack, the spring melt season, as modeled here, is accelerated and shortened due to the increase in net radiation created by the shrubs. This is similar to the findings in the observational study by *Sturm et al.* [2005]. *Chapin et al.* [2005] suggest a lengthening of the snow-free season, not believed to be directly related to current shrub coverage, has lead to warmer summer temperatures in northern Alaska. A further lengthening of the snow-free season, owing to increased shrubs, could enhance this warming even more.

[46] The shrubs, which are typically much taller than the lichens and mosses of the tundra, are capable of protruding through the snowpack earlier in the melt season. The dark protruding shrubs absorb incoming solar radiation much more efficiently than the high albedo snow and warm to higher temperatures. The relatively warm shrubs then emit longwave radiation to the snow and turbulent sensible heat flux to the surrounding air. The longwave radiation emitted by the shrubs is readily absorbed by the snow, a near blackbody. In addition, the warming of the air above the snow by the shrubs allows for warming of the snowpack through turbulent sensible heat transfer. The shrubs thus convert incoming shortwave radiation, a form of energy poorly absorbed by snow, to longwave radiation and sensible heat, forms which are readily absorbed by snow. In our model these warming effects more than offset the reduction of shortwave radiation by shading during the primary melt period. However, it should be noted that recent observations by *Pomeroy et al.* [2006] in the Yukon Territory show the melt period is longer in shrub areas despite the larger melt rates. The observations were made in shrubs with heights of 1–3 m while those in the simulation were given an average height of 0.75 m. It is possible that the taller shrubs in the observational study trapped more snow during the winter and produced a stronger shading effect during the melt period than the shorter shrubs in this simulation, enabling the snow to persist longer despite the faster rate of melt.

[47] According to our model, the reduction of snow albedo by soot deposition also leads to enhanced snow ablation during the melt season. The soot allows the snowpack to absorb more of the incoming solar radiation directly. However, soot appears to have relatively less influence on sensible heat flux and air temperatures since, unlike in the case of shrubs, the surface is limited to the freezing point. The temperature of polluted snow only exceeds that of clean snow when the ambient temperature is well below freezing and solar radiation is strong.

[48] We did not attempt to run a simulation with combined shrub and soot effects. Our goal in this study was to determine the relative influence of each effect on the model atmosphere and snowpack. Since the signs of all the values are the same for soot and shrub perturbations, the combined effect will likely be an amplification above and beyond the individual effects. The effects on snow melt and air temperatures presented here show that future changes in shrub distribution and soot pollution in the Arctic need to be accounted for in long-term simulations of climate. In addition, the changes in air temperature and snowmelt are large enough that they would likely be significant for smaller perturbations in shrub coverage and soot than those presented in this study.

5. Conclusions

[49] The modeling work described in this paper helps to show the significance of the shrub and soot effects at a

Table 2. Mean Difference Due to Shrubs and Soot with 99.9% Confidence Interval

Response Variable	Shrub Control	Soot Control
3-m air temperature, °C	2.2 ± <0.1	1.0 ± <0.1
Sensible heat flux, W m^{-2}	16.8 ± 0.1	2.3 ± <0.1
Latent heat flux, W m^{-2}	10.1 ± 0.1	1.6 ± < 0.1
Net radiation, W m^{-2}	28.4 ± 0.2	22.8 ± 0.2
Planetary boundary layer height, m	108 ± 1	25 ± 1
Snow melt rate, cm h^{-1}	0.004 ± 0.002	0.002 ± 0.002
Snow-free date, d	11 ± 1	5 ± <1

regional scale. By showing the importance of these processes with relatively little computational expense at the regional scale the importance of including such effects in long-term global climate simulations can be determined. In this study RAMS 4.4 was used to simulate the effects of a shrub invasion and soot deposition on snow melt and near-surface air temperature in the Kuparuk Basin of Alaska. First, control simulations spanning the tundra snowmelt period from May through late June for 3 a were run using the present day vegetation distribution and clean snow. The results of these simulations were compared with available observations to see how well the model could simulate reality. Last, two perturbation simulations were run, one with most of the present day tundra replaced with shrubs and another with present day vegetation but snow polluted with soot. The model estimated the snow melting off 11 d earlier in the shrub enhanced and 5 d earlier in the polluted snow run. According to the model, near-surface air temperatures averaged 2.2 and 1.0°C warmer during the snowmelt period in the shrub enhanced and polluted snow simulations, respectively. In addition, the model estimates planetary boundary layer heights averaged 108 m deeper in the shrub-enhanced simulation and 25 m deeper in the polluted snow simulation.

[50] **Acknowledgments.** We would like to thank Michael Coughenour, Richard Eykholt, and Christopher Hiemstra for their helpful suggestions and comments during the preparation of the Ph.D. dissertation chapters from which this manuscript was derived. In addition, we extend gratitude to three anonymous reviewers who provided many helpful suggestions. This work was supported by NASA Headquarters under the Earth System Science Fellowship grant NGT5-30527. Additional support was provided by NSF grant 0229973 and NASA grant NNG04GPS9G.

References

Armstrong, R. L., M. J. Brodzik, K. Knowles, and M. Savoie (2005), Global monthly EASE-Grid snow water equivalent climatology, http://www.nsidc.org/data/nsidc-0271.html, Natl. Snow and Ice Data Cent., Boulder, Colo.

Baker, D. G., D. L. Ruschy, and D. B. Wall (1990), The albedo decay of prairie snows, *J. Appl. Meteorol.*, *29*, 179–187.

Baker, D. G., D. L. Ruschy, R. H. Skaggs, and D. B. Wall (1992), Air temperature and radiation depression associated with a snow cover, *J. Appl. Meteorol.*, *31*, 247–254.

Chapin, F. S., III, W. Eugster, J. P. McFadden, A. H. Lynch, and D. A. Walker (2000), Summer differences among Arctic ecosystems in regional climate forcing, *J. Clim.*, *13*, 2002–2010.

Chapin, F. S., III, et al. (2005), Role of land-surface changes in Arctic summer warming, *Science*, *310*, 657–660.

Chen, C., and W. R. Cotton (1983), A one-dimensional simulation of the stratocumulus-capped mixed layer, *Boundary Layer Meteorol.*, *25*, 289–321.

Cohen, J., and D. Rind (1991), The effect of snow cover on the climate, *J. Clim.*, *4*, 689–706.

Cotton, W. R., et al. (2003), RAMS 2001: Current status and future directions, *Meteorol. Atmos. Phys.*, *82*, 5–29.

Dickinson, R. E., A. Henderson-Sellers, P. J. Kennedy, and M. F. Wilson (1986), Biosphere-Atmosphere Transfer Scheme (BATS) for the NCAR Community Climate Model, *Tech. Rep. NCAR/TN-275+STR*, Natl. Cent. for Atmos. Res., Boulder, Colo.

Douville, H., J.-F. Royer, and J.-F. Mahfouf (1995), A new snow parameterization for the Meteo-France climate model. Part I: Validation in stand alone experiments, *Clim. Dyn.*, *12*, 21–35.

Eastman, J. L., M. B. Coughenour, and R. A. Pielke Sr. (2001), The regional effects of CO_2 and landscape change using a coupled plant and meteorological model, *Global Change Biol.*, *7*, 797–815.

Ellis, A. W., and D. J. Leathers (1998), A quantitative approach to evaluating the effects of snow cover on cold airmass temperatures across the U.S. Great Plains, *Weather Forecast.*, *13*, 688–701.

Food and Agriculture Organization (1997), Digital soil map of the world and derived soil properties version 3.5, Rome.

Goetz, S. J., A. G. Bunn, G. J. Fiske, and R. A. Houghton (2005), Satellite-observed photosynthetic trends across boreal North America associated with climate and fire disturbance, *Proc. Natl. Acad. Sci. U.S.A.*, *102*, 13,521–13,525.

Hansen, J., and L. Nazarenko (2004), Soot climate forcing via snow and ice albedos, *Proc. Natl. Acad. Sci. U.S.A.*, *101*, 423–428.

Kalnay, E., et al. (1996), The NCEP/NCAR 40-year reanalysis project, *Bull. Am. Meteorol. Soc.*, *77*, 437–471.

Kane, D. L., and L. D. Hinzman (2005), Climate data from the North Slope Hydrology Research project, Univ. of Alaska Fairbanks Water and Environ. Res. Cent., Fairbanks, 9 September. (Available at http://www.uaf.edu/water/projects/NorthSlope/)

Kane, D. L., R. E. Gieck, and L. D. Hinzman (1997), Snowmelt modeling at small Alaskan Arctic watershed, *J. Hydrol. Eng.*, *2*, 204–210.

Keyser, D., and R. A. Anthes (1977), The applicability of a mixed-layer model of the planetary boundary layer to real-data forecasting, *Mon. Weather Rev.*, *105*, 1351–1371.

König, M., and M. Sturm (1998), Mapping snow distribution in the Alaskan Arctic using air photos and topographic relationships, *Water Resour. Res.*, *34*, 3471–3483.

Leathers, D. J., and D. A. Robinson (1993), The association between extremes in North American snow cover extent and United States temperatures, *J. Clim.*, *6*, 1345–1355.

Liston, G. E. (2004), Representing subgrid snow cover heterogeneities in regional and global models, *J. Clim.*, *17*, 1381–1397.

Liston, G. E., and M. Sturm (1998a), A snow-transport model for complex terrain, *J. Glaciol.*, *44*, 498–516.

Liston, G. E., and M. Sturm (1998b), Global seasonal snow classification system, http://www.nsidc.org/data/arcss045.html, Natl. Snow and Ice Data Cent., Boulder, Colo.

Liston, G. E., and M. Sturm (2002), Winter precipitation patterns in Arctic Alaska determined from a blowing-snow model and snow-depth observations, *J. Hydrometeorol.*, *3*, 646–659.

Liston, G. E., R. A. Pielke Sr., and E. M. Greene (1999), Improving first-order snow-related deficiencies in a regional climate model, *J. Geophys. Res.*, *104*, 19,559–19,567.

Liston, G. E., J. P. McFadden, M. Sturm, and R. A. Pielke Sr. (2002), Modelled changes in arctic tundra snow, energy and moisture fluxes due to increased shrubs, *Global Change Biol.*, *8*, 17–32.

Mellor, G. L., and T. Yamada (1982), Development of a turbulence closure model for geophysical fluid problems, *Rev. Geophys.*, *20*, 851–875.

Mendez, J., L. D. Hinzman, and D. L. Kane (1998), Evapotranspiration from a wetland complex on the arctic coastal plain of Alaska, *Nordic Hydrol.*, *29*, 303–330.

Mesinger, F., et al. (2006), North American regional reanalysis, *Bull. Am. Meteorol. Soc.*, *87*, 343–360.

Muller, S. V., A. E. Racoviteanu, and D. A. Walker (1999), Landsat MSS-derived land-cover map of northern Alaska: Extrapolation methods and a comparison with photo-interpreted and AVHRR-derived maps, *Int. J. Remote Sens.*, *20*, 2921–2946.

Namias, J. (1985), Some empirical evidence for the influence of snow cover on temperature and precipitation, *Mon. Weather Rev.*, *113*, 1542–1553.

Narapusetty, B., and N. Mölders (2005), Evaluation of snow depth and soil temperatures predicted by the Hydro-Thermodynamic Soil-Vegetation scheme coupled with the Fifth-Generation Pennsylvania State University-NCAR Mesoscale Model, *J. Appl. Meteorol.*, *44*, 1827–1843.

Olson, J. S. (1994a), Global ecosystem framework-definitions, USGS EROS Data Center internal report, 37 pp., U.S. Geol. Surv., Sioux Falls, S. D.

Olson, J. S. (1994b), Global ecosystem framework-translation strategy, USGS EROS Data Center internal report, 39 pp., U.S. Geol. Surv., Sioux Falls, S. D.

Otterman, J., M. D. Novak, and D. O. C. Starr (1993), Turbulent heat transfer from a sparsely vegetated surface: Two-component representation, *Boundary Layer Meteorol.*, *64*, 409–420.

Pielke, R. A., Sr. (2002), *Mesoscale Meteorological Modeling*, 2nd ed., *Int. Geophys. Ser.*, vol. 78, edited by R. Dmowska, J. R. Holton, and H. T. Rossby, 676 pp., Academic, San Diego, Calif.

Pielke, R. A., and Y. Mahrer (1978), Verification analysis of the University of Virginia three-dimensional mesoscale model prediction over south Florida for July 1, 1973, *Mon. Weather Rev.*, *106*, 1568–1589.

Pomeroy, J. W., D. S. Bewley, R. L. H. Essery, N. R. Hedstrom, T. Link, R. J. Granger, J. E. Sicart, C. R. Ellis, and J. R. Janowicz (2006), Shrub tundra snowmelt, *Hydrol. Proc.*, *20*, 923–941.

Segal, M., and R. A. Pielke (1981), Numerical model simulation of human biometeorological heat load conditions—Summer day case study for the Chesapeake Bay area, *J. Appl. Meteorol.*, *20*, 735–749.

Shaw, B. L., R. A. Pielke, and C. L. Ziegler (1997), A three-dimensional numerical simulation of a Great Plains dryline, *Mon. Weather Rev.*, *125*, 1489–1506.

Smagorinsky, J. (1963), General circulation experiments with the primitive equations. Part I. The basic experiment, *Mon. Weather Rev.*, *91*, 99–164.

Strack, J. E., R. A. Pielke Sr., and J. Adegoke (2003), Sensitivity of model-generated daytime surface heat fluxes over snow to land-cover changes, *J. Hydrometeorol.*, *4*, 24–42.

Strack, J. E., G. E. Liston, and R. A. Pielke Sr. (2004), Modeling snow depth for improved simulations of snow-vegetation-atmosphere interactions, *J. Hydrometeorol.*, *5*, 723–734.

Sturm, M., C. Racine, and K. Tape (2001a), Increasing shrub abundance in the Arctic, *Nature*, *411*, 546–547.

Sturm, M., J. P. McFadden, G. E. Liston, F. S. Chapin III, C. H. Racine, and J. Holmgren (2001b), Snow-shrub interactions in Arctic tundra: A hypothesis with climate implications, *J. Clim.*, *14*, 336–344.

Sturm, M., T. Douglas, C. Racine, and G. E. Liston (2005), Changing snow and shrub conditions affect albedo with global implications, *J. Geophys. Res.*, *110*, G01004, doi:10.1029/2005JG000013.

Tape, K., M. Sturm, and C. Racine (2006), The evidence for shrub expansion in Northern Alaska and the Pan-Arctic, *Global Change Biol.*, *12*, 686–702.

Verseghy, D. L. (1991), CLASS—a Canadian land surface scheme for GCMS. 1. Soil model, *Int. J. Climatol.*, *11*, 111–133.

Walko, R. L., et al. (2000), Coupled atmosphere-biophysics-hydrology models for environmental modeling, *J. Appl. Meteorol.*, *39*, 931–944.

G. E. Liston, Cooperative Institute for Research in the Atmosphere, Colorado State University, Fort Collins, CO 80523, USA.

R. A. Pielke Sr. and J. E. Strack, Cooperative Institute for Research in the Environmental Sciences, University of Colorado, Boulder, CO 80309, USA. (jstrack@cires.colorado.edu)